

Time-varying Parameter Tensor Vector Autoregression

Yiyong Luo Jim E. Griffin

Department of Statistical Science, University College London, WC1E 6BT, UK

ABSTRACT

Time-varying parameter vector autoregression provides a flexible framework to capture structural changes within time series. However, when applied to high-dimensional data, this model encounters challenges of over-parametrization and computational burden. We address these challenges by building on recently proposed Tensor VAR models to represent the time-varying coefficient matrix as a third-order tensor with CANDECOMP/PARAFAC (CP) decomposition, yielding three model configurations where different sets of components are specified as time-varying, each offering distinct interpretations. To select the model configuration and the decomposition rank, we evaluate multiple variants of Deviance Information Criterion (DIC) corresponding to the conditional and marginal DICs. Our simulation demonstrates that a specific conditional DIC variant provides more reliable results and accurately identifies true model configurations. We improve the accuracy of rank selection by applying knee point detection to the DICs, rather than defaulting to the minimum DIC value. Upon analyzing functional magnetic resonance imaging data from story reading tasks, our selected model configurations suggest time-varying dynamics while reducing the number of parameters by over 90% relative to standard VARs. Granger causality analysis reveals directional brain connectivity patterns that align with narrative progression, with various regions functioning as signal emitters or receivers at different time points.

Keywords: time-varying parameter vector autoregression, tensor, Deviance information criterion, Granger causality, fMRI

1 Introduction

Time-varying parameter vector autoregression (TVP-VAR) is a multivariate time series model where coefficients evolve gradually according to random walks. Since its introduction in macroeconomics (Cogley and Sargent, 2001, 2005; Primiceri, 2005), TVP-VAR has become a methodological cornerstone in the field due to its ability to capture structural changes both flexibly and robustly (Nakajima, 2011). Beyond macroeconomics, TVP-VAR has been successfully applied in neuroscience (Havlicek et al., 2010) and finance (Geraci and Gnabo, 2018), where time series data exhibit non-stationarity.

Applications of TVP-VARs to high-dimensional time series are challenging due to over-parameterization and computational burden. Consequently, empirical studies typically employ fewer than 10 variables to mitigate these issues. To retain the high-dimensional structure of the data, two strands have emerged in the literature. The first strand employs well-designed priors to maintain model parsimony. Belmonte et al. (2014), Prüser (2021), Eisenstat et al. (2016) and Huber et al. (2021) formulated TVP-VARs using the non-centered parameterization (Frühwirth-Schnatter and Wagner, 2010) and imposed shrinkage priors to both time-invariant parameters and the error terms governing time-varying dynamics. Chan (2023) assigned a Bernoulli variable to each parameter to determine whether it should be modeled dynamically or remain static. The second strand implements dimension reduction techniques to decrease the number of unknown parameters. Korobilis (2013) compressed high-dimensional data to low-dimensional factors and modeled these factors with a TVP-VAR. Similarly, Chan et al. (2020) and Fischer et al. (2023) reduced the parameter space by adopting factor-like structures to time-varying parameters. Brune et al. (2022) and Cubadda et al. (2025) proposed time-varying extensions of reduced-rank VAR (Carriero et al., 2011) and multivariate autoregressive index model (Reinsel, 1983), respectively.

Our work falls within the second strand using dimension reduction, where we develop a time-varying parameter tensor VAR (TVP-TVAR). Firstly introduced by Wang et al. (2022), tensor VAR (TVAR) expresses the time-invariant VAR coefficient matrix in terms of a third-order tensor and reduces the number of parameters via tensor decomposition. While Luo and Griffin (2025) and Chan and Qi (2024) have investigated Bayesian TVARs for modeling high-dimensional time series, their approaches focus on evolving variance-covariance matrices and static conditional mean. To leverage the advantage of TVARs within TVP-VARs, time-varying tensors would be necessary, yet research in this area remains scarce. Among the few existing studies, Harris et al. (2021) and Chen

[et al. \(2023\)](#) constructed the tensors with time corresponding to one dimension without explicitly specifying the time variation; [Zhang et al. \(2021\)](#) developed a model where a subset of elements within the tensor decomposition is active at each time point, controlled by a time-varying rank value - an unknown parameter in the decomposition.

In this paper, we define a TVP-TVAR with the time-varying tensor and provide methods for posterior inference and model selection. In particular, we decompose the third-order tensor via the CANDECOMP/PARAFAC (CP) decomposition ([Kiers, 2000](#)) with a fixed rank, which represents the tensor as a sum of products of *margins* (i.e. the elements in the tensor decomposition). The CP decomposition partitions margins into three *loadings*: response, predictor and temporal. The response loading explains how data connects with a representation of past information, formulated by the predictor and temporal loadings. Each row of the predictor (temporal) loading determines how a specific variable (lag) contributes to this representation. Our model assumes one loading to be time-varying while maintaining the other two as time-invariant, resulting in three configurations. Although incorporating multiple time-varying loadings is possible, we restrict our model to these three configurations as they provide distinct interpretations of how temporal dynamics manifest in relationships between time series and their lags. Additionally, modeling only one time-varying loading is computationally efficient. By specifying the evolution of time-varying margins as random walks, we can treat the TVP-TVAR as a state-space model, facilitating straightforward Bayesian inference.

The TVP-TVAR model requires selecting an appropriate configuration (from one time-invariant and three time-varying options) and a CP decomposition rank. While existing tensor-structured models generally do not need to select model configuration, various methods have been applied in rank selection. [Guhaniyogi and Spencer \(2021\)](#), [Billio et al. \(2023\)](#), [Luo and Griffin \(2025\)](#), and [Fana et al. \(2022\)](#), among others, imposed shrinkage priors to eliminate redundant margins, thereby decreasing the rank from an initialized maximum. Alternatively, [Zhou et al. \(2013\)](#), [Li and Zhang \(2017\)](#), [Li et al. \(2018\)](#) and [Spencer et al. \(2022\)](#), to name a few, employed information criteria, such as Bayesian information criterion ([Schwarz, 1978](#)) and Deviance information criterion (DIC) ([Spiegelhalter et al., 2002](#)), to determine the optimal rank. Given the prevalence of DIC in Bayesian analysis and its capacity to simultaneously select both configuration and rank with computational efficiency, we adopt DIC for model selection.

Since the TVP-TVAR represents a state-space model with time-varying parameters being latent variables, several DIC variants established in latent variable models are available for model selection

(Celeux et al., 2006). Choosing an appropriate DIC variant has received increasing attention in time series research (Chan and Grant, 2016b; Chan and Eisenstat, 2018; Li et al., 2020) and other statistical domains (Ariyo et al., 2020, 2022; Merkle et al., 2019). We compare two types of DICs extensively investigated in the literature: conditional and marginal DICs. The conditional DIC evaluates the likelihood conditional on latent variables, while marginal DIC integrates them out. We specify two conditional and one marginal DICs based on the TVP-TVAR framework. While most references mentioned favor the marginal DIC due to concerns about uncertainty and complexity bias in conditional DICs, our simulation study reveals that one particular conditional DIC demonstrates advantages for TVP-TVARs — it yields more reliable results measured by lower Monte Carlo errors compared to alternative DICs, and accurately identifies the true model configuration. Based on these findings, we opt for this conditional DIC for model selection. Although higher ranks lead to lower chosen DICs, the improvement diminishes gradually as the rank increases, aligning with the finding in Maity et al. (2021) that DIC distinguishes underfitted models but not overfitted ones. Thus, instead of determining the rank corresponding to the minimum DIC, we implement the "kneedle" algorithm (Satopaa et al., 2011) to a sequence of DICs across ranks for knee point detection, which improves the performance of identifying the optimal rank.

We demonstrate the utility of TVP-TVARs using functional magnetic resonance imaging (fMRI) data sets collected by Wehbe et al. (2014) from multiple subjects while reading a chapter in *Harry Potter and the Sorcerer's Stone* (Rowling, 2012). The result from model selection indicates that the dynamics of the fMRI data are time-varying, which reflects the conclusion of Gaschler-Markefski et al. (1997) about the non-stationarity of the fMRI data. The CP decompositions with selected ranks manage to reduce the number of parameters by over 90%, relative to standard VARs. The Granger causality analysis from the selected model shows that the number of directional brain connectivity is consistent with the narrative progression. Different regions of interest function as primary signal emitters or receivers at various time points.

The rest of the paper is organized as follows. Section 2 specifies the model framework. Section 3 describes the posterior sampler of unknown parameters. Section 4 discusses DIC variants and details our implementation of the "kneedle" algorithm. A Monte Carlo study in Section 5 supports one of the conditional DICs for model selection. Section 6 provides the empirical results of applying TVP-TVARs to the fMRI data.

2 Methodology

2.1 Tensor VAR

A time-invariant tensor VAR with lag order P , denoted as TVAR(P), uses a third-order tensor to store the coefficients in a VAR. In particular, the mathematical expression is written as

$$\mathbf{y}_t = \mathbf{A}_1 \mathbf{y}_{t-1} + \dots + \mathbf{A}_P \mathbf{y}_{t-P} + \boldsymbol{\epsilon}_t, \quad (2.1)$$

$$= \mathcal{A}_{(1)} \mathbf{x}_t + \boldsymbol{\epsilon}_t, \quad (2.2)$$

where $\mathbf{y}_t \in \mathbb{R}^N$ denotes the multivariate data of interest at time point t , $\mathbf{x}_t = (\mathbf{y}'_{t-1}, \dots, \mathbf{y}'_{t-P})' \in \mathbb{R}^{NP}$ represents the P lags of \mathbf{y}_t , $\mathcal{A} \in \mathbb{R}^{N \times N \times P}$ is the third-order tensor, with $\mathcal{A}_{i_1, i_2, p}$ corresponding to the (i_1, i_2) entry in $\mathbf{A}_p \in \mathbb{R}^{N \times N}$, for $i_1, i_2 = 1, \dots, N$ and $p = 1, \dots, P$, $\mathcal{A}_{(1)} = (\mathbf{A}_1, \dots, \mathbf{A}_P) \in \mathbb{R}^{N \times NP}$ is the mode-1 matricization of \mathcal{A} , see Appendix A for the definition.

TVAR is especially useful in modeling high-dimensional time series because it can reduce the number of parameters via tensor decomposition. Among the tensor decompositions reviewed in [Kolda and Bader \(2009\)](#), we employ CANDECOMP/PARAFAC (CP) decomposition ([Kiers, 2000](#)) in this paper due to its simplicity. Specifically, the CP decomposition of \mathcal{A} is given by

$$\mathcal{A} = \sum_{r=1}^R \mathcal{A}^{(r)} = \sum_{r=1}^R \boldsymbol{\beta}_1^{(r)} \circ \boldsymbol{\beta}_2^{(r)} \circ \boldsymbol{\beta}_3^{(r)}, \quad (2.3)$$

where R is the decomposition rank, $\mathcal{A}^{(r)}$ is a third-order tensor with dimensions identical to \mathcal{A} , for $r = 1, \dots, R$. The vectors $\boldsymbol{\beta}_1^{(r)}, \boldsymbol{\beta}_2^{(r)} \in \mathbb{R}^N$ and $\boldsymbol{\beta}_3^{(r)} \in \mathbb{R}^P$ are called *margins*, which form $\mathcal{A}^{(r)}$ through an outer product such that the (i_1, i_2, i_3) entry in $\mathcal{A}^{(r)}$ equals to $\boldsymbol{\beta}_{1, i_1}^{(r)} \boldsymbol{\beta}_{2, i_2}^{(r)} \boldsymbol{\beta}_{3, i_3}^{(r)}$ for $i_1, i_2 = 1, \dots, N$ and $i_3 = 1, \dots, P$ (see Appendix A for the definition of outer product). We denote the CP decomposition in (2.3) as $\mathcal{A} = \llbracket \mathbf{B}_1, \mathbf{B}_2, \mathbf{B}_3 \rrbracket_{\text{CP}}$, where $\mathbf{B}_j = (\boldsymbol{\beta}_j^{(1)}, \dots, \boldsymbol{\beta}_j^{(R)}) \in \mathbb{R}^{I_j \times R}$ is referred to as *loadings*, for $j = 1, 2, 3$, $I_1 = I_2 = N$ and $I_3 = P$. With an upper bound $R < N^2 P / (2N + P)$, the number of parameters decreases from $N^2 P$ in \mathcal{A} to $(2N + P)R$ in $\mathbf{B}_1, \mathbf{B}_2$ and \mathbf{B}_3 . Thus, when considering the coefficient matrix alone, TVAR allows parameters to increase linearly with the number of variables rather than quadratically, as in standard VAR models. This low-rank structure in the CP decomposition introduces parsimony, alleviating the over-parameterization issue commonly encountered when analyzing high-dimensional time series.

The three loadings in the CP decomposition constitute the interpretation of a TVAR. Recall that [Wang et al. \(2022\)](#) and [Luo and Griffin \(2025\)](#) referred to $\mathbf{B}_1, \mathbf{B}_2$ and \mathbf{B}_3 as response, predictor and temporal loadings, respectively. The terminology reflects their functional roles, and [Luo and Griffin](#)

(2025) provided a detailed discussion of these roles. To summarize: each row of the response loading explains how an individual variable in \mathbf{y}_t connects to a representation of past information, $\mathbf{B}'_2 \mathbf{X}_t \mathbf{B}_3$, where $\mathbf{X}_t = (\mathbf{y}_{t-1}, \dots, \mathbf{y}_{t-p})$; while each row of the predictor (temporal) loading determines how a specific variable (lag) contributes to this representation.

2.2 Time-varying Parameter Tensor VAR

We incorporate temporal dynamics into \mathcal{A} to formulate a time-varying parameter TVAR (TVP-TVAR)

$$\mathbf{y}_t = \mathcal{A}_{t,(1)} \mathbf{x}_t + \boldsymbol{\epsilon}_t, \quad \boldsymbol{\epsilon}_t \sim \mathcal{N}(\mathbf{0}, \boldsymbol{\Omega}), \quad (2.4)$$

where $\mathcal{A}_{t,(1)} = \mathbf{A}_t = (\mathbf{A}_{t,1}, \dots, \mathbf{A}_{t,p})$ corresponds to the mode-1 matricization of the time-varying tensor \mathcal{A}_t . We define three CP decompositions of \mathcal{A}_t with the ranks being fixed over time: (1) $\mathcal{A}_t = \llbracket \mathbf{B}_{t,1}, \mathbf{B}_2, \mathbf{B}_3 \rrbracket_{\text{CP}}$, (2) $\mathcal{A}_t = \llbracket \mathbf{B}_1, \mathbf{B}_{t,2}, \mathbf{B}_3 \rrbracket_{\text{CP}}$, (3) $\mathcal{A}_t = \llbracket \mathbf{B}_1, \mathbf{B}_2, \mathbf{B}_{t,3} \rrbracket_{\text{CP}}$. Each decomposition sets one loading as time-varying while keeping the other two time-invariant. We refer to a TVP-TVAR with P lags and the j -th loading being time-varying as TVP-TVAR(P, j), for $j = 1, 2, 3$.

While the CP decomposition can include more than one time-varying loading, we restrict it to the above three configurations mainly because each of them offers a distinct interpretation of how temporal dynamics manifest in the relationships between \mathbf{y}_t and its lags. Extended from the interpretation of loadings in a TVAR, TVP-TVAR($P, 1$) models a static construction of the past information, but the response of \mathbf{y}_t to the past information evolves over time. Conversely, TVP-TVAR($P, 2$) and ($P, 3$) operate under the opposite framework: the transformation of lagged values into the representation of past information varies temporally, while the relationship between \mathbf{y}_t and this representation is fixed. In particular, these two decompositions allow time-varying effects from individual variables or lags to the representation. Two additional considerations support our focus on TVP-TVAR(P, j): identifiability constraints and computational efficiency. Regarding identifiability, Remark 1 establishes the identifiability conditions for the margins¹. Notably, incorporating multiple time-varying loadings in the CP decomposition would cause both scaling and permutation transformations to be time-dependent, posing challenges in comparing model configurations.

¹ While margins in TVP-TVAR(P, j) are non-identifiable, the composite tensor formed by these margins maintains identifiability (Zhou et al., 2013; Guhaniyogi et al., 2017; Zhang et al., 2021).

Remark 1 TVP-TVAR(P, j) is identified up to scaling and permutation. Taking TVP-TVAR($P, 1$) as an example. $\mathcal{A}_t = \llbracket \mathbf{B}_{t,1}, \mathbf{B}_2, \mathbf{B}_3 \rrbracket_{\text{CP}} = \llbracket \tilde{\mathbf{B}}_{t,1}, \tilde{\mathbf{B}}_2, \tilde{\mathbf{B}}_3 \rrbracket_{\text{CP}}$, if loadings in the second CP decomposition satisfies:

1. Scaling: $\tilde{\mathbf{B}}_{t,1} = \mathbf{B}_{t,1} \mathbf{R}_1$, and $\tilde{\mathbf{B}}_{j'} = \mathbf{B}_{j'} \mathbf{R}_{j'}$, for $j' = 2$ and 3 . \mathbf{R}_j is an R -by- R diagonal matrix with $\prod_{j=1}^3 \mathbf{R}_{j,(r,r)} = 1$ for $r = 1, \dots, R$, where $\mathbf{R}_{j,(r,r)}$ is the r -th diagonal term in \mathbf{R}_j .
2. Permutation: $\tilde{\mathbf{B}}_{1,t} = \mathbf{B}_{1,t} \mathbf{\Pi}$ and $\tilde{\mathbf{B}}_{j'} = \mathbf{B}_{j'} \mathbf{\Pi}$, for $j = 2$ and 3 , and an arbitrary R -by- R column-wise permutation matrix $\mathbf{\Pi}$.

Margins in TVP-TVAR($P, 2$) and TVP-TVAR($P, 3$) are weakly identifiable under analogous conditions.

Throughout the rest of this paper, we denote the time-varying loading in TVP-TVAR (P, j) as $\mathbf{B}_{t,j}$ and the time-invariant ones as $\mathbf{B}_{j'}$ for $j', j \in \{1, 2, 3\}$ and $j' \neq j$. Following the standard structure in TVP-VAR (Primerici, 2005), we model the evolution of $\mathbf{b}_{t,j} = \text{vec}(\mathbf{B}_{t,j})$, for $t = 2, \dots, T$, as a random walk

$$\mathbf{b}_{t,j} = \mathbf{b}_{t-1,j} + \boldsymbol{\eta}_{t,j}, \quad \boldsymbol{\eta}_{t,j} \sim \mathcal{N}(\mathbf{0}, \mathbf{Q}_j), \quad (2.5)$$

where $\mathbf{Q}_j = \text{diag}(q_{j,1}, \dots, q_{j,I_j R})$ is a diagonal matrix, for $I_1, I_2 = N$, $I_3 = P$, $q_{j,k}$ follows an inverse-gamma prior, $\mathcal{IG}(a_k, b_k)^2$, for $k = 1, \dots, I_j R$. We impose normal priors to $\mathbf{b}_{1,j}$ and $\mathbf{b}_{j'} = \text{vec}(\mathbf{B}_{j'})$, $\mathcal{N}(\mathbf{0}, \boldsymbol{\Sigma}_j)$ and $\mathcal{N}(\mathbf{0}, \boldsymbol{\Sigma}_{j'})$, respectively. Following the spirit of Minnesota-type prior (Litterman et al., 1979), which posits that the shorter lags contain more information than longer

lags, we specify $\boldsymbol{\Sigma}_j = \begin{cases} \sigma^2 \mathbf{I}_{NR}, & j = 1 \text{ or } 2 \\ \sigma^2 \mathbf{I}_R \otimes \text{diag}\left(1, \frac{1}{2^2}, \dots, \frac{1}{p^2}\right), & \text{otherwise} \end{cases}$, where \mathbf{I}_{NR} and \mathbf{I}_R are identity

matrices with dimensions specified in their subscripts³. $\boldsymbol{\Sigma}_{j'}$, the variance-covariance matrix of $\mathbf{b}_{j'}$ share the same expression. $\boldsymbol{\Sigma}_3$ imposes an increasing shrinkage property to \mathbf{B}_3 (or the initialization of $\mathbf{B}_{t,3}$), wherein the shrinkage level increases with the loading row index, thereby prioritizing information from shorter lags over longer lags in the past information representation. These margin priors imply that the (i_1, i_2, p) entry of the tensor initialization, decomposed by $\mathbf{B}_{1,j}$ and $\mathbf{B}_{j'}$'s, has zero mean and variance $R\sigma^6/p^2$. Finally, $\boldsymbol{\Omega}$ follows an inverse-Wishart prior, $\boldsymbol{\Omega} \sim \mathcal{IW}(\nu, \mathbf{S})^4$.

² If a random variable x follows $\mathcal{IG}(a, b)$, its probability density function is $\frac{b^a}{\Gamma(a)} (1/x)^{a+1} \exp(-b/x)$, where $\Gamma(\cdot)$ is the gamma function.

³ Note that $\boldsymbol{\Sigma}_j$, for $j = 1$ or 2 , does not need to include estimated standard deviations like a Minnesota-type prior when the data is standardized.

⁴ If an n -by- n positive definite matrix \mathbf{Q} follows $\mathcal{IW}(\nu, \mathbf{S})$, where ν is a scalar and $\mathbf{S} \in \mathbb{R}^{n \times n}$, then its probability density function is $\frac{|\mathbf{S}|^{\nu/2}}{2^{n\nu/2} \Gamma_n(\nu/2)} |\mathbf{Q}|^{-\frac{\nu+n+1}{2}} e^{-\frac{1}{2} \text{tr}(\mathbf{S}\mathbf{Q}^{-1})}$, where Γ_n is the multivariate gamma function.

Two points are noteworthy if the time-varying margins follow random walks as defined in (2.5). First, if σ^2 is a known parameter, margins are identifiable up to sign switching and permutation, instead of scaling and permutation described as in Remark 1. This is because if the two CP decompositions in Remark 1 provide the same tensor and satisfy the scaling condition, then $\tilde{\mathbf{b}}_{1,j} = \text{vec}(\tilde{\mathbf{B}}_{1,j})$ follows a multivariate normal distribution with zero mean and variance-covariance matrix $(\mathbf{R}_j \otimes \mathbf{I}_{I_j}) \boldsymbol{\Sigma}_j (\mathbf{R}_j \otimes \mathbf{I}_{I_j})'$, which equals to $\boldsymbol{\Sigma}_j$ only when diagonal entries in \mathbf{R}_j are 1 or -1. The same explanation also applies to margins in the time-invariant loadings, $\mathbf{B}_{j'}$. According to Luo and Griffin (2025), the scaling indeterminacy of the CP decomposition is one of the sources of high autocorrelation in the MCMC samples of margins. To mitigate high autocorrelation from this source, we assume σ^2 to be known. Second, TVP-TVAR(P, j) implies that the VAR coefficients evolve as random walks, which leads to a state-space representation

$$\mathbf{y}_t = (\mathbf{I}_N \otimes \mathbf{x}'_t) \mathbf{a}_t + \boldsymbol{\epsilon}_t, \quad \mathbf{a}_t = \mathbf{a}_{t-1} + \boldsymbol{\xi}_t, \quad (2.6)$$

where $\mathbf{a}_t = \text{vec}(\mathbf{A}'_t)$. Suppose the model is TVP-TVAR($P, 1$), then $\boldsymbol{\xi}_{t,i}$ (for $i = 1, \dots, N^2P$) is independent to other elements in $\boldsymbol{\xi}_t$ and follow $\mathcal{N}\left(0, \sum_{r=1}^R (\mathbf{B}_{2,(i_2,r)})^2 (\mathbf{B}_{3,(i_3,r)})^2 q_{1,(r-1)+i_1}\right)$, for $i = NP(i_1 - 1) + N(i_3 - 1) + i_2$, where $\mathbf{B}_{j',(i_j',r)}$ is the (i_j', r) entry of $\mathbf{B}_{j'}$, for $i_1, i_2 = 1, \dots, N$ and $i_3 = 1, \dots, P$. If the model is TVP-TVAR($P, 2$) or TVP-TVAR($P, 3$), one can change the three terms in the normal distribution accordingly.

3 Posterior Computation

We now turn to the MCMC algorithm to estimate unknown parameters in (2.4) and (2.5) given the priors specified in the previous section and a fixed rank R . We adopt a Gibbs sampler to sample $\{\mathbf{b}_{1:T,j}, \mathbf{b}_{j'}, \mathbf{Q}_j, \boldsymbol{\Omega}\}$. The sampler cycles through the following steps.

Step 1. We sample $\mathbf{b}_{1:T,j}$ using the forward filtering backward sampling algorithm (Frühwirth-Schnatter, 1994; Carter and Kohn, 1994). This approach is feasible because, analogous to the rearrangements in TVARs, see Wang et al. (2022), TVP-TVAR(P, j) can be rearranged as

$$\mathbf{y}_t = \mathbf{Z}_{t,j} \mathbf{b}_{t,j}^* + \boldsymbol{\epsilon}_t \quad (3.1)$$

where $\mathbf{Z}_{t,1} = (\mathbf{x}'_t (\mathbf{B}_3 \otimes \mathbf{B}_2) \mathcal{I}'_{(1)}) \otimes \mathbf{I}_N$, $\mathbf{Z}_{t,2} = \mathbf{B}_1 \mathcal{I}_{(1)} ((\mathbf{B}'_3 \mathbf{X}'_t) \otimes \mathbf{I}_R)$, $\mathbf{Z}_{t,3} = \mathbf{B}_1 \mathcal{I}_{(1)} (\mathbf{I}_R \otimes (\mathbf{B}'_2 \mathbf{X}_t))$, $\mathcal{I} \in \mathbb{R}^{R \times R \times R}$ is a superdiagonal tensor with ones on non-zero entries (the definition of superdiagonal tensor is in Appendix A), $\mathbf{b}_{t,j}^* = \mathbf{b}_{t,j}$ for $j = 1$ and 3 , $\mathbf{b}_{t,2}^* = \text{vec}(\mathbf{B}'_{t,2})$. Incorporating this equation with the random walk of $\mathbf{b}_{t,j}$ yields a linear state-space model.

Step 2. $\mathbf{b}_{j'}$ comprises two blocks corresponding to loading specified in the previous section, with each block having similar full conditionals. Based on (3.1), the full conditionals of $\mathbf{b}_{j'}$, for $j' = 1$ or 3, or that of $\mathbf{b}_{j'}^*$, for $j = 2$, is $\mathcal{N}(\bar{\boldsymbol{\mu}}_{j'}, \bar{\boldsymbol{\Sigma}}_{j'})$ with

$$\bar{\boldsymbol{\Sigma}}_{j'}^{-1} = \boldsymbol{\Sigma}_{j'}^{-1} + \sum_{t=1}^T \mathbf{Z}'_{t,j'} \boldsymbol{\Omega}^{-1} \mathbf{Z}_{t,j'}, \quad \bar{\boldsymbol{\mu}}_{j'} = \bar{\boldsymbol{\Sigma}}_{j'} \sum_{t=1}^T \mathbf{Z}'_{t,j'} \boldsymbol{\Omega}^{-1} \mathbf{y}_t,$$

where \mathbf{B}_j in $\mathbf{Z}_{t,j'}$ changes to $\mathbf{B}_{t,j}$.

Step 3. The by-product of samples from Step 1 and 2 is the time-varying tensor \mathcal{A}_t . The variance-covariance matrix $\boldsymbol{\Omega}$ is sampled given $\mathcal{A}_{t,(1)}$ and $\mathbf{y}_{1:T}$ from

$$\mathcal{IW} \left(T + \nu, \sum_{t=1}^T (\mathbf{y}_t - \mathcal{A}_{t,(1)} \mathbf{x}_t) (\mathbf{y}_t - \mathcal{A}_{t,(1)} \mathbf{x}_t)' + \mathbf{S} \right).$$

Step 4. Sample $q_{j,k}$, for $k = 1, \dots, I_j R$, from

$$\mathcal{IG} \left(a_k + \frac{T}{2}, b_k + \frac{1}{2} \sum_{t=2}^T (\mathbf{b}_{t,j,k} - \mathbf{b}_{t-1,j,k})^2 \right),$$

where $\mathbf{b}_{t,j,k}$ is the k -th element in $\mathbf{b}_{t,j}$.

4 Model Selection

Given the TVP-TVAR framework and a data set, we need to select a model configuration to describe the time variation of loadings and a rank value. There are 4 configurations corresponding to TVAR(P) and TVP-TVAR(P, j), for $j = 1, 2, 3$, and we select the rank from 1 to R^* , a pre-defined upper bound. While existing tensor-structured models generally do not select model configuration, rank selection has been extensively investigated. [Guhaniyogi et al. \(2017\)](#) and [Luo and Griffin \(2025\)](#) imposed shrinkage priors to margins with a rank of R^* and shrank the rank by removing redundant margins from the model. This approach requires only one MCMC simulation, rather than multiple simulations with different rank values, thus enhancing computational efficiency; however, given the complexity of the TVP-TVAR, we opt not to impose any additional shrinkage prior. Alternatively, one can select an evaluation metric and incrementally increase the rank from 1 until the metric no longer indicates improvement in model performance. One advantage of this approach compared to imposing shrinkage priors mentioned is that we can select both model configuration and rank simultaneously. Several evaluation metrics are available for model selection, including Bayes factor (BF) ([Jeffreys, 1935](#)) and Deviance information criterion (DIC) ([Spiegelhalter et al., 2002](#)). The DIC offers practical advantages, as it can be more readily evaluated from MCMC outputs compared

to the BF⁵. Given the widespread adoption of DIC in both Bayesian time series (Chan and Grant, 2016b; Chan and Eisenstat, 2018; Bai and Wang, 2015; Li et al., 2020) and tensor-structured models (Guhaniyogi and Spencer, 2021; Spencer et al., 2022), we use this metric for model selection.

To facilitate further discussion about DIC, we briefly introduce it in the TVP-TVAR framework. The deviance of parameter θ , $D(\theta)$, is defined as $D(\theta) = -2 \log p(\mathbf{y}_{1:T} | \theta) + 2 \log h(\mathbf{y}_{1:T})$, where $h(\mathbf{y}_{1:T})$ is a fully-specified standardizing term which only depends on $\mathbf{y}_{1:T}$. The DIC balances goodness-of-fit and model complexity by a summation of two terms

$$\text{DIC}(\theta) = \overline{D(\theta)} + p_D,$$

where $\overline{D(\theta)} = -2 \mathbb{E}_\theta (\log p(\mathbf{y}_{1:T} | \theta)) + 2 \log h(\mathbf{y}_{1:T})$ is the posterior mean deviance and p_D denotes the effective number of parameters. In particular, p_D is the difference between posterior mean deviance and deviance of posterior mean, $\overline{D(\theta)} - D(\hat{\theta})$. Since $h(\mathbf{y}_{1:T})$ is independent of θ , one can set $h(\mathbf{y}_{1:T})$ as 1 and write the DIC as

$$\text{DIC}(\theta) = -4 \mathbb{E}_\theta (\log p(\mathbf{y}_{1:T} | \theta)) + 2 \log p(\mathbf{y}_{1:T} | \hat{\theta}), \quad (4.1)$$

where we approximate the first term by the MCMC samples of θ and plug the sample mean $\hat{\theta}$ into the second term.

Since the TVP-TVAR can be written as state-space models, as described in (2.6) and (3.1), $\mathcal{A}_{1:T}$ and $\mathbf{b}_{t,j}$ serve as latent variables in these two respective equations. Following Celeux et al. (2006), if θ includes latent variables, we regard the DIC in (4.1) as conditional DIC because the likelihood is conditional on these latent variables. This conditional DIC has two variants based on the specification of θ . The first variant, denoted as $\text{DIC}^{c,1}$, is formulated with $\theta = \{\mathcal{A}_{1:T}, \Omega\}$. The second variant, $\text{DIC}^{c,2}$, corresponds to the specification where $\theta = \{\mathbf{b}_{1:T,j}, \mathbf{b}_{j'}, \Omega\}$. These two variants are distinct due to the difference in their deviances of posterior mean, $p(\mathbf{y}_{1:T} | \hat{\theta})$. Specifically, both conditional DIC variants need to compute the time-varying tensor based on $\hat{\theta}$. Take the TVP-TVAR($P, 1$) as an example, these tensors correspond to $\mathbb{E}[\llbracket \mathbf{B}_{t,1}, \mathbf{B}_2, \mathbf{B}_3 \rrbracket_{\text{CP}}]$ and $\llbracket \mathbb{E}[\mathbf{B}_{t,1}], \mathbb{E}[\mathbf{B}_2], \mathbb{E}[\mathbf{B}_3] \rrbracket_{\text{CP}}$ in $\text{DIC}^{c,1}$ and $\text{DIC}^{c,2}$, respectively, and these expressions can differ because the loadings may have posterior correlation. An alternative DIC widely studied in latent variable models is marginal DIC, denoted as DIC^m , which takes the form of (4.1) with $\theta = \{\mathbf{b}_{j'}, \mathbf{Q}_j, \Omega\}$. This DIC marginalizes $\mathcal{A}_{1:T}$ and $\mathbf{b}_{1:T,j}$ in $\text{DIC}^{c,1}$ and $\text{DIC}^{c,2}$, respectively, and uses an integrated likelihood $p(\mathbf{y}_{1:T} | \theta) = \int p(\mathbf{y}_{1:T} | \mathcal{A}_{1:T}, \Omega) p(\mathcal{A}_{1:T} | \mathbf{b}_{j'}, \mathbf{Q}_j) d\mathcal{A}_{1:T} =$

⁵ Beyond the scope of this paper, the DIC has additional advantages over BF. Notably, the latter suffers Jeffreys–Lindley paradox (see detailed description in Robert (2014)) and is not well-defined with improper priors, i.e. the corresponding marginal likelihood is arbitrary up to a multiplicative constant, whereas the former does not have these issues.

$\int p(\mathbf{y}_{1:T} | \mathbf{b}_{1:T,j}, \mathbf{b}_{j'}, \boldsymbol{\Omega}) p(\mathbf{b}_{1:T,j} | \mathbf{b}_{j'}, \mathbf{Q}_j) d\mathbf{b}_{1:T,j}$ to evaluate model performance. A closed form expression for $\log p(\mathbf{y}_{1:T} | \boldsymbol{\theta})$ is available in Appendix B.

Various studies favor marginal DIC over conditional ones for two reasons. Firstly, conditional DICs potentially exhibits more uncertainty than marginal DIC since it depends on the latent variables (Chan and Grant, 2016a; Merkle et al., 2019). Secondly, the conditional DICs tend to choose the most complex model even if the data generating process is less complex (Millar, 2009; Chan and Grant, 2016a). However, we show that the concern about the first limitation can be invalid without a specific condition, and the second limitation of conditional DICs can be addressed by knee point detection.

For the first limitation about the uncertainty of DICs, we emphasize that this uncertainty stems from the posterior uncertainty of $\boldsymbol{\theta}$. Due to the indeterminacy of the CP decomposition, as discussed in Remark 1, margins defined in Section 2.2 are identifiable up to sign switching and permutation, resulting in highly autocorrelated margin Markov chains⁶. The consequence of this autocorrelation is that margins present high sample variance within a single MCMC simulation, and their sample means exhibit high variation given multiple simulations (see Figure 2, 3 and 4 in the next section for an illustration). $\text{DIC}^{c,1}$ and DIC^m , which incorporate margins, inherently demonstrate greater uncertainty compared to $\text{DIC}^{c,1}$, whose parameters of interest do not suffer from this indeterminacy issue. Therefore, we prefer $\text{DIC}^{c,1}$ for model selection.

We regard the model complexity about the second limitation in two facets: model configuration and rank choice. For the former, TVP-TVAR(P , 1) and TVP-TVAR(P , 2) are more complex due to more parameters included relative to those in TVP-TVAR(P , 3) and time-invariant TVAR. According to the Monte Carlo study about $\text{DIC}^{c,1}$ in Section 5, this conditional DIC does not favor a more complex model configuration over the one that generates the data. Next, we move to the rank choice. While higher ranks do yield lower $\text{DIC}^{c,1}$, the model improvement gradually diminishes when the rank exceeds a certain value, based on the simulation results in the next section (see Figure 1a). This reflects the finding in Maity et al. (2021) that the DIC tends to distinguish underfitted models but not overfitted models⁷. Therefore, a useful tool to prevent $\text{DIC}^{c,1}$ from choosing the highest available rank is knee point detection, which detects the point of maximum curvature in a function.

⁶ Although the autocorrelation arising from the scaling indeterminacy has been mitigated, autocorrelation due to sign switching and permutation still occurs.

⁷ The DIC described in Maity et al. (2021) corresponds to (4.1), but it cannot be considered as the conditional DIC because their model does not have any latent structure.

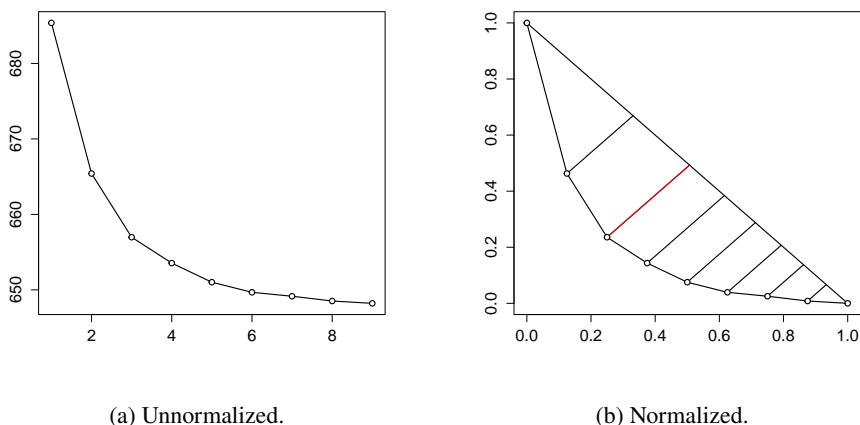


Figure 1: Example of unnormalized (left) and normalized (right) conditional DICs (presented in circles) computed from the data set generated from TVP-TVAR(3, 1) with a rank of 3. The straight lines connecting the circles and $y = -x + 1$ represent the distance between them, with the red line representing the maximum distance.

Multiple definitions of maximum curvature result in different algorithms for knee point detection. For example, [Zhao et al. \(2008\)](#) defined an angle-based curvature to select the number of clusters using a Bayesian information criterion curve; [Satopaa et al. \(2011\)](#) proposed "kneedle" to find the maximum distance between a normalized curve and a straight line (the detailed definition will be provided). We choose "kneedle" for knee point detection because it has a clearer visualization of maximum curvature and gives higher accuracy in detecting knees compared to the angle-based one. Specifically, locating the maximum curvature in a discrete sequence $\text{DIC}_{\mathcal{M}}^{c,1} = (\text{DIC}_{\mathcal{M},1}^{c,1}, \dots, \text{DIC}_{\mathcal{M},R^*}^{c,1})$, which stores the $\text{DIC}^{c,1}$'s with model configuration \mathcal{M} and different rank values, involves two steps. The first step is to normalize each conditional DIC to $\widetilde{\text{DIC}}_{\mathcal{M},R}^{c,1} = (\text{DIC}_{\mathcal{M},R}^{c,1} - \text{DIC}_{\mathcal{M},R_{\min}}^{c,1}) / (\text{DIC}_{\mathcal{M},R_{\max}}^{c,1} - \text{DIC}_{\mathcal{M},R_{\min}}^{c,1})$, where R_{\min} and R_{\max} represent the ranks associated with the minimum and maximum DICs, and convert the corresponding rank R to $(R - 1) / (R^* - 1)$. The curve in Figure 1b represents these normalized DICs computed using the simulation data in Section 5. Then, we identify the point with the maximum curvature as that with the maximum distance to the line which passes points $(0, \widetilde{\text{DIC}}_{\mathcal{M},1}^{c,1})$ and $(1, \widetilde{\text{DIC}}_{\mathcal{M},R^*}^{c,1})$. As illustrated in Figure 1b, this maximum curvature occurs at the third point, so we select the rank as 3, which is the true rank value defined in the next section.

5 A Monte Carlo Study

5.1 Data and Implementation

This section demonstrates the utility of $DIC^{c,1}$ (henceforth referred to as DIC for brevity) in model selection. We generate 100 3-variable datasets from each of four model configurations: TVAR(3), TVP-TVAR(3, j), for $j = 1, 2, 3$. Each data set contains 200 observations and the corresponding tensors are generated from CP decompositions with a rank of 3. We set σ^2 , the multiplier in the margin variance, as 0.5, resulting in prior variances of 0.375, 0.094, and 0.042 for the coefficients in A_1, A_2, A_3 (or their corresponding initializations in time-varying models), respectively. Ω is sampled from the inverse-Wishart distribution stated in Section 2.2, with $\nu = 6$ and $S = I_3$, so that the prior mean of Ω is $0.5I_3$. Q_j , the variance-covariance matrix in the random walk process of time-varying margins, is a diagonal matrix with all non-zero element being 0.01.

With $N = P = 3$, the maximum rank that can be selected is 9, as $R \leq \{N^2, NP\}$ (Kolda and Bader, 2009). Therefore, there are 36 (9×4) possible models to select from for each data set. We estimate parameters in TVP-TVAR models using the algorithm described in Section 3, while for TVAR models, we modify Step 2 in the algorithm to incorporate three blocks of loadings rather than two, followed by implementation of the remaining two steps in the algorithm. To compute the DIC of each model and data set, we run 10 parallel Markov chains, each having 10,000 iterations with 1,000 burn-in. Following parameter estimation, we calculate the DIC for knee point detection by averaging the DIC from each of the 10 runs. The "kneedle" algorithm then helps determine the rank choice for each of the four model configurations. After recording the four corresponding DICs, we select the model configuration with the lowest value.

5.2 Simulation Result

First, we compare the Monte Carlo errors corresponding to all the DIC variants mentioned in Section 4, and show the reason why we prefer $DIC^{c,1}$. The Monte Carlo error of a data set is calculated as the sample standard deviation of the 10 DICs obtained from the 10 parallel MCMC runs. A lower Monte Carlo error indicates that the corresponding DIC variant is more reliable because it has lower uncertainty. As illustrated in Figure 2a, most Monte Carlo errors of $DIC^{c,1}$ are below 1, whereas those in Figure 2b and 2c range from 0 to 500, with at most 10 being smaller than 1. These findings support our decision to use $DIC^{c,1}$ for model selection in the TVP-TVAR framework.

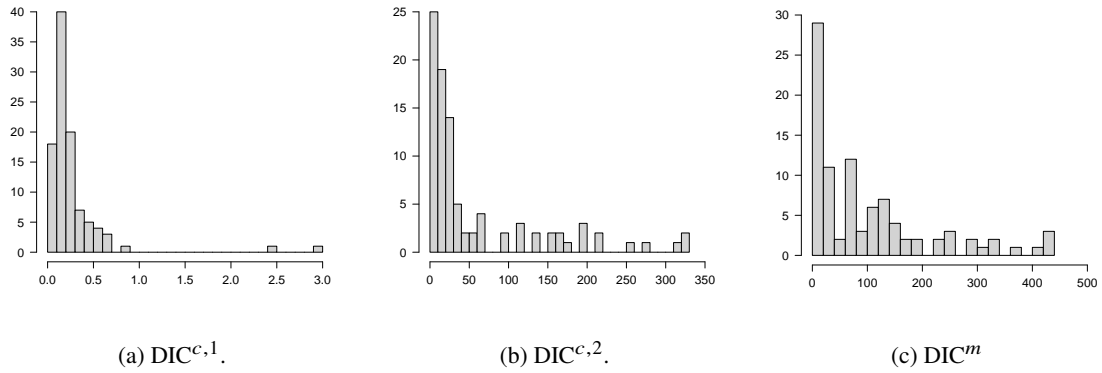


Figure 2: Histograms of Monte Carlo errors of conditional and marginal DICs, computed using data sets generated from TVP-TVAR(3, 1). The model configuration and rank associated with these DICs align with the true data generating process. The middle and right panels restrict the display of Monte Carlo errors to a maximum of 350 and 500, respectively, which accounts for 93 data sets. Each Monte Carlo error is scaled by $1/\sqrt{10}$ for visualization clarity.

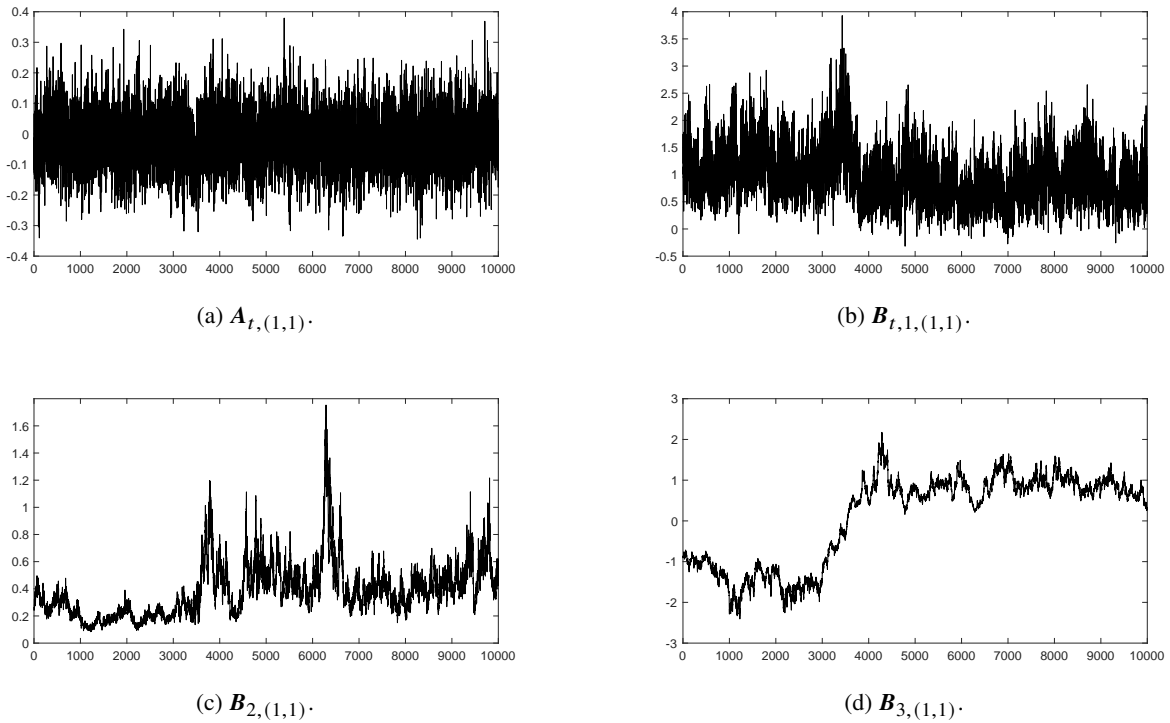


Figure 3: Trace plots of coefficients and margins sampled using TVP-TVAR(3,1) with a rank of 3.

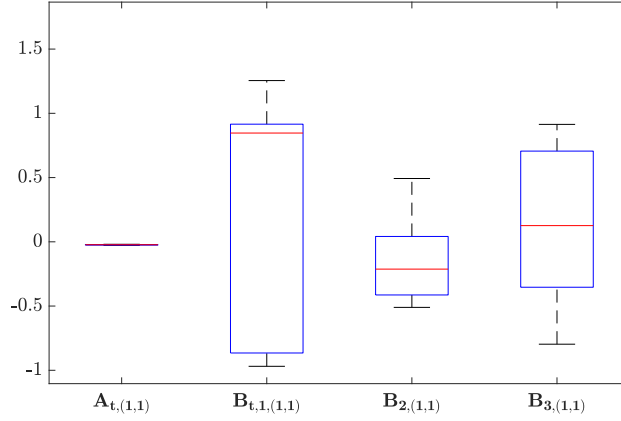


Figure 4: Boxplots of sample mean of coefficients and margins across 10 MCMC runs for the inference of one data set, generated from TVP-TVAR(3,1) with a rank of 3.

Figure 3 and 4 explain why $DIC^{c,1}$ is more reliable than other DICs. Figure 3 presents the trace plots of the (1,1)-entry in the coefficient matrix A_t alongside its decomposed margins - the (1,1) entry in $B_{t,1}$, B_2 and B_3 - at time point $t = 100$. One can also use (1,2) or (1,3) entries in the loadings for demonstration. These trace plots show that the Markov chain of the coefficient mixes well, whereas the margin ones have higher autocorrelation which cannot be solved by thinning. Notably, the sample variance of the coefficient is much lower than those margin counterparts. This autocorrelation, stemming from the indeterminacy of the CP decomposition, also elevates uncertainty of margin sample mean, as presented in Figure 4. This figure depicts boxplots of sample means of these parameters examined in Figure 3. Each boxplot displays 10 data points, with each point representing a sample mean derived from one MCMC run. The indeterminacy of the CP decomposition can result in loadings sampled from different MCMC runs representing permuted and sign-switched versions of the same underlying margins. To prevent this phenomenon from distorting our results, we aligned margins across parallel MCMC runs using correlation matching. Specifically, we compute correlations between the (1,1) entry samples shown in Figure 3 and the (1, r) entry samples of the same loading in other runs, for $r = 1, 2, 3$. The matching process identifies margins by selecting those with the highest absolute correlation, then adjusts them by multiplying with the sign of the correlation. Figure 4 demonstrates that the boxplot of coefficient sample mean exhibits lower variation compared to the margin counterparts. Since these sample means serve as plug-in parameters ($\hat{\theta}$) in deviance of posterior mean, $DIC^{c,1}$ yields more reliable results by incorporating coefficient sample means compared to $DIC^{c,2}$ and DIC^m , which use margin sample means.

Next, we illustrate that the DIC can identify true model configurations. Table 1 presents the confusion matrix of configuration selection. Applying DICs enables the correct identification of model configurations in nearly all cases. TVAR is only selected when it is the true configuration. When the true configuration involves time-varying parameters, only a handful of data sets are misclassified. While Millar (2009) and Chan and Grant (2016b) showed that the conditional DIC favors complex models in their simulation studies, we do not reach the same conclusion here. For example, TVAR and TVP-TVAR(3,3) are relatively less complex compared to the other two configurations, but the model selection of the former two attains over 90% accuracy.

		Selected			
		TVAR(3)	TVP-TVAR(3,1)	TVP-TVAR(3,2)	TVP-TVAR(3,3)
True	TVAR(3)	96	0	2	2
	TVP-TVAR(3,1)	0	97	2	1
	TVP-TVAR(3,2)	0	8	89	3
	TVP-TVAR(3,3)	0	3	4	93

Table 1: Confusion matrix of configuration selection.

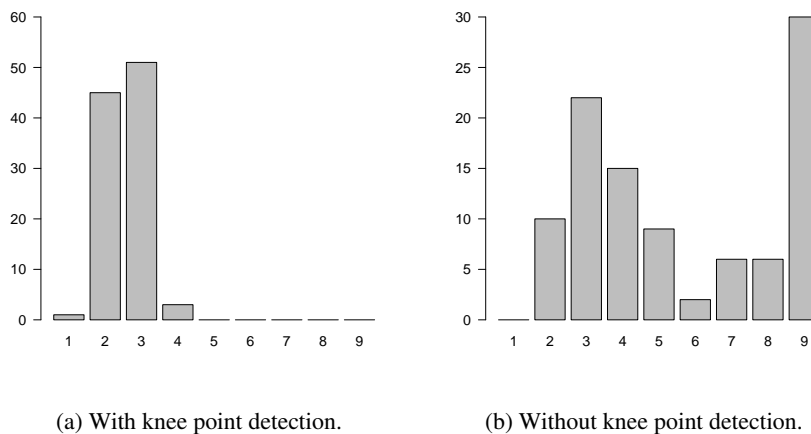


Figure 5: Histograms of selected ranks based on the data sets generated from TVP-TVAR(3,1).

Lastly, we show that the knee point detection improves rank selection. Figure 5 depicts the distributions of selected ranks if the data is generated from TVP-TVAR(3,1). We record ranks determined using the knee point detection in the left panel and select the ranks corresponding to the lowest DICs in the right panel. According to the left panel, DICs with knee point detection correctly identify the true rank ($R = 3$) in over 50 data sets, with almost all remaining data sets selecting ranks adjacent to the true rank (i.e. $R = 2$ or $R = 4$). In contrast, ranks selected without the knee point detection span from 2 to 9, with $R = 9$ having the highest frequency. This suggests that knee point

detection alleviates the tendency of DICs to favor overfitted models. Similar conclusions emerge from analysis using other model configurations (see figures in Appendix C).

6 Empirical Results

6.1 Data and Implementation

We apply TVP-TVARs to a functional magnetic resonance imaging (fMRI) data set about story understanding (Wehbe et al., 2014) to study the time variation of brain connectivity. The data was collected from 8 subjects when reading chapter 9 of *Harry Potter and the Sorcerer’s Stone* (Rowling, 2012). All subjects are native English speakers and right-handed individuals who are familiar with the story in the chapter. The subject read the chapter in rapid serial visual format, i.e. the token was presented one by one for 0.5 seconds each. The chapter contains approximately 5,200 tokens and was divided into four runs, each lasting approximately 11 minutes. Before and after each run, there would be 20-second and 10-second breaks, respectively, for the subject to stare at a cross on the screen. For each subject in each run, the fMRI data was collected per two seconds from 21764 voxels, corresponding to 117 regions of interest (ROIs).

Following Zhang et al. (2021) and Xiong and Cribben (2023), we select $N = 27$ ROIs which control various cognitive and sensory functions (see the ROIs selected in Appendix D). For each ROI, we take the average of the voxel data within this particular ROI to form one time series. We discard the data when subjects took breaks and split the time series according to the runs. This process yields 32 (number of subjects \times number of runs) data sets, with each in the format of $T_{\text{run id}} \times 27$ (the average value of $T_{\text{run id}}$ is 323). We then standardize each data set to avoid any scaling issue.

Following the lag order in Zhang et al. (2021), we apply TVAR(4), TVP-TVAR(4, j), for $j = 1, 2, 3$, to the data sets and select the rank from 1 to 10, extending beyond the rank of 8 previously reported as sufficiently large in Zhang et al. (2021). For the margin prior, we set $\sigma^2 = 0.1$, which leads to the variance range of coefficients in A_p in TVAR or $A_{1,p}$ in TVP-TVAR as $\frac{1}{p^2} \times [10^{-3}, 10^{-2}]$, for $p = 1, \dots, 4$, given the rank range. The inverse-Wishart prior of the variance-covariance matrix has parameters $\nu = N + 3$ and $S = \mathbf{I}_N$. We set $a_k = b_k = 0.01$ so that non-zero elements in \mathbf{Q}_j have non-informative inverse-gamma priors.

6.2 Model Selection

We first demonstrate the model selection using one data set corresponding to Subject 1 reading the first part of the chapter. Then, we move to a summary of model selection using all 32 data sets. Table 2 presents the DICs computed with a range of model configurations and ranks. Overall, the DICs corresponding to TVP-TVAR(4,1) are lower than those of other configurations with the same rank value. The rank is selected to be 5 or 6 across configurations, as indicated in bold in the table. By comparing these 4 DICs in bold, we select TVP-TVAR(4,1) as the model configuration with a rank of 6. This suggests that Subject 1, when reading the first part of the chapter, had ROIs that processed information from past signals dynamically and maintained a static framework for gathering information from these signals.

Model	$R = 1$	$R = 2$	$R = 3$	$R = 4$	$R = 5$	$R = 6$	$R = 7$	$R = 8$	$R = 9$	$R = 10$
TVAR(4)	7290.70	6660.44	6171.06	5705.06	5300.59	4977.97	4746.89	4542.20	4375.59	4243.74
TVP-TVAR(4,1)	6645.54	6096.65	5560.65	5145.82	4762.24	4449.99	4309.18	4162.92	4031.85	3909.93
TVP-TVAR(4,2)	7280.87	6637.43	6120.45	5690.45	5276.53	4941.90	4697.56	4467.36	4291.59	4115.15
TVP-TVAR(4,3)	7335.64	6781.22	6319.24	5880.49	5529.93	5299.88	5024.46	4793.37	4657.43	4590.32

Table 2: DICs evaluated from the data for which Subject 1 read the first part of the chapter. DICs corresponding to the knee points are in bold.

We repeat the same analysis to all 32 data sets, and summarize the results in Figure 6. Three-quarters of the datasets favor TVP-TVAR(4,1), meaning that VAR coefficients exhibit temporal variation due to evolving signal reception patterns across ROIs. The three TVAR selections correspond to Subject 3 or the first part of the chapter, while TVP-TVAR(4,2) is only selected when the subjects read the second and third parts. None of the data sets identify TVP-TVAR(4,3) as the optimal model fit. Based on these selected ranks, predominantly 4 and 5, Table 3 summarizes the average parameter counts for both standard VARs and TVARs. It reveals that both TVAR and TVP-TVARs effectively reduce the number of parameters by over 90%, inducing parsimonious model structures. Due to the high computational cost in standard VARs, we do not fit the data using these models in the application.

6.3 Granger Causality Analysis

Granger causality is a prevalent analysis in neuroscience to identify directional connectivity patterns between brain regions (Seth et al., 2015). To demonstrate Granger causality analysis using TVP-TVAR, we use the data set of Subject 1 reading the first part. The model implemented is

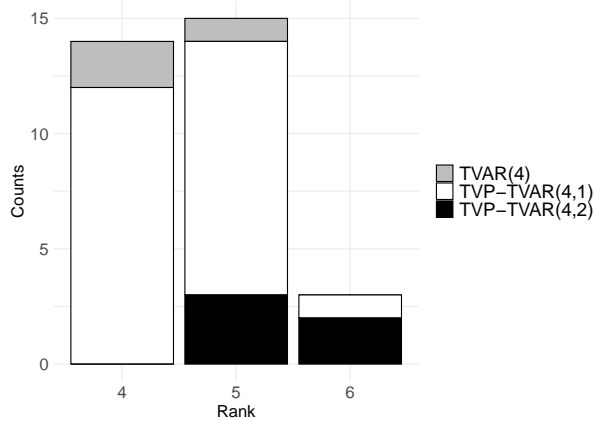


Figure 6: Counts of models selected across 32 data sets.

TVP-TVAR(4,1) with a rank of 6, selected according to Table 2. The results of other data sets are available upon request.

Informally, Granger causality from time series m to n exists when forecasts of time series n are more accurate by including time series m in the model compared to excluding it. A VAR defines the existence of Granger causality from time series m to n as whether the (n, m) entry in $A_{t,p}$, for $p = 1, \dots, P$, are non-zero. If all the associated coefficients are zeros, then time series m does not Granger cause time series n . Since Bayesian inference of VARs rarely estimates coefficients as exact zeros without specific priors, such as spike-and-slab prior (Mitchell and Beauchamp, 1988), we define time series m Granger causes n at time t if $p_{t,(m \rightarrow n)} = p(|A_{t,p,(n,m)}| > \delta \text{ for any } p = 1, \dots, P \mid y_{1:T})$ is higher than a threshold p^* , where we set δ as 0.01 following Fana et al. (2022) and p^* as 99.9% to limit the false positive connections.

Figure 7 depicts the number of Granger causalities detected over time. When the subject started reading, there were relatively limited connections between brain regions. Subsequently, the connections increased progressively, maintaining levels above 90 across time points after $t=100$. This pattern of Granger causality is related to the narrative progression in the first part of the chapter. For example, connectivity peaks during a pivotal scene featuring Harry and his friends participating in their first flying lesson. The number of Granger causalities begins to decline around $t = 225$ as the narrative focus shifts away from the protagonists.

To illustrate the evolving connectivity patterns of ROIs, we rank $p_{t,(m \rightarrow n)}$ at a particular time point t in descending order and display the first 50 connections for visualization. Figure 8 provides the Granger causality networks at $t = 1, 171$ and 300, corresponding to the start of the chapter, Harry

Standard VARs		Tensor VARs	
VAR	2916	TVAR(4)	251
TVP-VAR	941139	TVP-TVAR(4,1)	39718
		TVP-TVAR(4,2)	47224
		TVP-TVAR(4,3)	/

Table 3: Averaged number of parameters estimated across all subjects and runs based on different configurations.

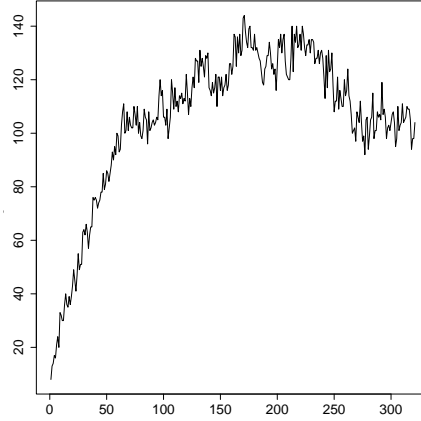


Figure 7: Granger causality time series

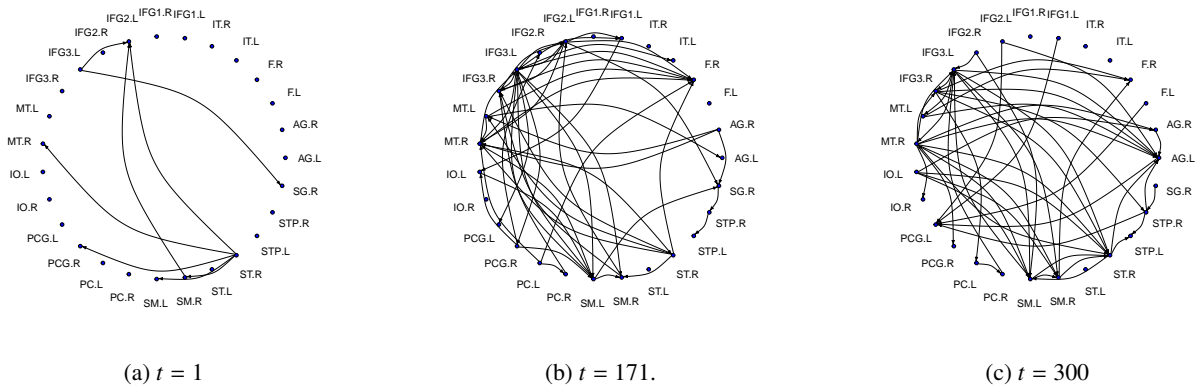


Figure 8: Granger causality networks at different time points.

started his flying lesson and the accident of Nievell, respectively. In Figure 8a, ST.R (right superior temporal gyrus) emitted the majority of signals. This region plays an important role in receptive language function and social cognition (Bigler et al., 2007), indicating that the subject began to process the textual information of this chapter, which involves numerous character interactions. The network became denser in Figure 8b as the story progressed to the flying lesson. The ROI receiving the highest number of signals (7) from other ROIs is the right fusiform gyrus (F.R), which specializes in high-level visual processing functions, including reading and object recognition (Weiner and Zilles, 2016). Compared to Figure 8a, 17 additional connections originated from the inferior frontal gyrus areas (nodes prefixed with IFG), which is a multifunctional region with functionalities including, but not limited to, speech perception, programming sequential order of motor executions and social interaction (Liakakis et al., 2011). This pattern aligns with findings reported in Zhang et al. (2021), who showed similar shifts in Granger causality patterns during another key scene in the chapter. Moving to Figure 8c, the left angular gyrus (AG.L) and the right superior temporal gyrus

(ST.R), which are both related to auditory processing (Seghier, 2013; Bigler et al., 2007), not only received more signals than other ROIs but also exhibited the most notable changes compared to the previous figure. In particular, AG.L and ST.R received 9 and 6 signals, respectively, increasing from 1 at $t = 171$. A possible explanation for this increase in signals received is that the corresponding story segment involves more auditory elements, such as teacher instructions and laughter, compared to other story segments.

7 Conclusion and Discussion

We propose the time-varying parameter tensor vector autoregression with three model configurations and implement a conditional DIC with knee point detection for model selection. The fMRI data application demonstrates that time variation in the response loading is the preferred configuration for most subjects. This finding supports the non-stationarity of fMRI data and reveals time-varying dynamics between the data and its representation of past information.

Our work can be extended in several directions. First, it would be interesting to incorporate TVP-TVARs with shrinkage priors to allow a hybrid model analogous to the VAR counterpart proposed in Chan (2023). One caveat is the identifiability issue of the margins, which could hinder sampling and interpretation. Second, developing techniques for obtaining convergent margin Markov chains can potentially lower the uncertainty in the alternative DICs specified in Section 4. Third, heteroskedasticity plays a critical role in VAR applications within econometrics (Clark and Mertens, 2023), suggesting that adding heteroskedasticity such as stochastic volatility to TVP-TVARs is worth investigating.

References

- Ariyo, O., Lesaffre, E., Verbeke, G., and Quintero, A. (2022). Model selection for Bayesian linear mixed models with longitudinal data: sensitivity to the choice of priors. *Communications in Statistics-simulation and Computation*, 51(4):1591–1615.
- Ariyo, O., Quintero, A., Muñoz, J., Verbeke, G., and Lesaffre, E. (2020). Bayesian model selection in linear mixed models for longitudinal data. *Journal of Applied Statistics*, 47(5):890–913.
- Bai, J. and Wang, P. (2015). Identification and Bayesian estimation of dynamic factor models. *Journal of Business & Economic Statistics*, 33(2):221–240.
- Belmonte, M. A., Koop, G., and Korobilis, D. (2014). Hierarchical shrinkage in time-varying parameter models. *Journal of Forecasting*, 33(1):80–94.

- Bigler, E. D., Mortensen, S., Neeley, E. S., Ozonoff, S., Krasny, L., Johnson, M., Lu, J., Provencal, S. L., McMahon, W., and Lainhart, J. E. (2007). Superior temporal gyrus, language function, and autism. *Developmental Neuropsychology*, 31(2):217–238.
- Billio, M., Casarin, R., Iacopini, M., and Kaufmann, S. (2023). Bayesian dynamic tensor regression. *Journal of Business & Economic Statistics*, 41(2):429–439.
- Brune, B., Scherrer, W., and Bura, E. (2022). A state-space approach to time-varying reduced-rank regression. *Econometric Reviews*, 41(8):895–917.
- Carriero, A., Kapetanios, G., and Marcellino, M. (2011). Forecasting large datasets with Bayesian reduced rank multivariate models. *Journal of Applied Econometrics*, 26(5):735–761.
- Carter, C. K. and Kohn, R. (1994). On Gibbs sampling for state space models. *Biometrika*, 81(3):541–553.
- Celeux, G., Forbes, F., Robert, C. P., and Titterton, D. M. (2006). Deviance information criteria for missing data models. *Bayesian Analysis*, 1(4):651 – 673.
- Chan, J. C. (2023). Large hybrid time-varying parameter VARs. *Journal of Business & Economic Statistics*, 41(3):890–905.
- Chan, J. C. and Eisenstat, E. (2018). Bayesian model comparison for time-varying parameter VARs with stochastic volatility. *Journal of Applied Econometrics*, 33(4):509–532.
- Chan, J. C., Eisenstat, E., and Strachan, R. W. (2020). Reducing the state space dimension in a large TVP-VAR. *Journal of Econometrics*, 218(1):105–118.
- Chan, J. C. and Grant, A. L. (2016a). Fast computation of the deviance information criterion for latent variable models. *Computational Statistics & Data Analysis*, 100:847–859.
- Chan, J. C. and Grant, A. L. (2016b). On the observed-data deviance information criterion for volatility modeling. *Journal of Financial Econometrics*, 14(4):772–802.
- Chan, J. C. and Qi, Y. (2024). Large Bayesian Tensor VARs with stochastic volatility. *arXiv preprint arXiv:2409.16132*.
- Chen, X., Zhang, C., Chen, X., Saunier, N., and Sun, L. (2023). Discovering dynamic patterns from spatiotemporal data with time-varying low-rank autoregression. *IEEE Transactions on Knowledge and Data Engineering*, 36(2):504–517.
- Clark, T. E. and Mertens, E. (2023). Stochastic volatility in Bayesian vector autoregressions. Oxford University Press.
- Cogley, T. and Sargent, T. J. (2001). Evolving post-world war II US inflation dynamics. *NBER Macroeconomics Annual*, 16:331–373.

- Cogley, T. and Sargent, T. J. (2005). Drifts and volatilities: monetary policies and outcomes in the post WWII US. *Review of Economic dynamics*, 8(2):262–302.
- Cubadda, G., Grassi, S., and Guardabascio, B. (2025). The time-varying multivariate autoregressive index model. *International Journal of Forecasting*, 41(1):175–190.
- Eisenstat, E., Chan, J. C., and Strachan, R. W. (2016). Stochastic model specification search for time-varying parameter VARs. *Econometric Reviews*, 35(8-10):1638–1665.
- Fana, J., Sitekb, K., Chandrasekaranb, B., and Sarkara, A. (2022). Bayesian tensor factorized mixed vector autoregressive models for inferring Granger causality patterns from high-dimensional multi-subject panel neuroimaging data. *arXiv preprint arXiv:2206.10757*, 3.
- Fischer, M. M., Hauzenberger, N., Huber, F., and Pfarrhofer, M. (2023). General Bayesian time-varying parameter vector autoregressions for modeling government bond yields. *Journal of Applied Econometrics*, 38(1):69–87.
- Frühwirth-Schnatter, S. (1994). Data augmentation and dynamic linear models. *Journal of Time Series Analysis*, 15(2):183–202.
- Frühwirth-Schnatter, S. and Wagner, H. (2010). Stochastic model specification search for Gaussian and partial non-Gaussian state space models. *Journal of Econometrics*, 154(1):85–100.
- Gaschler-Markefski, B., Baumgart, F., Tempelmann, C., Schindler, F., Stiller, D., Heinze, H.-J., and Scheich, H. (1997). Statistical methods in functional magnetic resonance imaging with respect to nonstationary time-series: auditory cortex activity. *Magnetic Resonance in Medicine*, 38(5):811–820.
- Geraci, M. V. and Gnabo, J.-Y. (2018). Measuring interconnectedness between financial institutions with Bayesian time-varying vector autoregressions. *Journal of Financial and Quantitative Analysis*, 53(3):1371–1390.
- Guhaniyogi, R., Qamar, S., and Dunson, D. B. (2017). Bayesian tensor regression. *Journal of Machine Learning Research*, 18(79):1–31.
- Guhaniyogi, R. and Spencer, D. (2021). Bayesian tensor response regression with an application to brain activation studies. *Bayesian Analysis*, 16(4):1221–1249.
- Harris, K. D., Aravkin, A., Rao, R., and Brunton, B. W. (2021). Time-varying autoregression with low-rank tensors. *SIAM Journal on Applied Dynamical Systems*, 20(4):2335–2358.
- Havlicek, M., Jan, J., Brazdil, M., and Calhoun, V. D. (2010). Dynamic Granger causality based on Kalman filter for evaluation of functional network connectivity in fMRI data. *Neuroimage*, 53(1):65–77.

- Huber, F., Koop, G., and Onorante, L. (2021). Inducing sparsity and shrinkage in time-varying parameter models. *Journal of Business & Economic Statistics*, 39(3):669–683.
- Jeffreys, H. (1935). Some tests of significance, treated by the theory of probability. In *Mathematical Proceedings of the Cambridge Philosophical Society*, volume 31, pages 203–222. Cambridge University Press.
- Kiers, H. A. (2000). Towards a standardized notation and terminology in multiway analysis. *Journal of Chemometrics: A Journal of the Chemometrics Society*, 14(3):105–122.
- Kolda, T. G. and Bader, B. W. (2009). Tensor decompositions and applications. *SIAM review*, 51(3):455–500.
- Korobilis, D. (2013). Assessing the transmission of monetary policy using time-varying parameter dynamic factor models. *Oxford Bulletin of Economics and Statistics*, 75(2):157–179.
- Li, L. and Zhang, X. (2017). Parsimonious tensor response regression. *Journal of the American Statistical Association*, 112(519):1131–1146.
- Li, X., Xu, D., Zhou, H., and Li, L. (2018). Tucker tensor regression and neuroimaging analysis. *Statistics in Biosciences*, 10(3):520–545.
- Li, Y., Yu, J., and Zeng, T. (2020). Deviance information criterion for latent variable models and misspecified models. *Journal of econometrics*, 216(2):450–493.
- Liakakis, G., Nickel, J., and Seitz, R. (2011). Diversity of the inferior frontal gyrus—a meta-analysis of neuroimaging studies. *Behavioural Brain Research*, 225(1):341–347.
- Litterman, R. B. et al. (1979). Techniques of forecasting using vector autoregressions. Working Paper 115, Federal Reserve Bank of Minneapolis.
- Luo, Y. and Griffin, J. E. (2025). Bayesian inference of vector autoregressions with tensor decompositions. *Journal of Business & Economic Statistics*, 0(0):1–29.
- Maity, A. K., Basu, S., and Ghosh, S. (2021). Bayesian criterion-based variable selection. *Journal of the Royal Statistical Society Series C: Applied Statistics*, 70(4):835–857.
- Merkle, E. C., Furr, D., and Rabe-Hesketh, S. (2019). Bayesian comparison of latent variable models: Conditional versus marginal likelihoods. *Psychometrika*, 84(3):802–829.
- Millar, R. B. (2009). Comparison of hierarchical Bayesian models for overdispersed count data using DIC and Bayes’ factors. *Biometrics*, 65(3):962–969.
- Mitchell, T. J. and Beauchamp, J. J. (1988). Bayesian variable selection in linear regression. *Journal of the American Statistical Association*, 83(404):1023–1032.

- Nakajima, J. (2011). Time-Varying Parameter VAR Model with Stochastic Volatility: An Overview of Methodology and Empirical Applications. IMES Discussion Paper Series 11-E-09, Institute for Monetary and Economic Studies, Bank of Japan.
- Primiceri, G. E. (2005). Time varying structural vector autoregressions and monetary policy. *The Review of Economic Studies*, 72(3):821–852.
- Prüser, J. (2021). The horseshoe prior for time-varying parameter VARs and monetary policy. *Journal of Economic Dynamics and Control*, 129:104188.
- Reinsel, G. (1983). Some results on multivariate autoregressive index models. *Biometrika*, 70(1):145–156.
- Robert, C. P. (2014). On the Jeffreys-Lindley paradox. *Philosophy of Science*, 81(2):216–232.
- Rowling, J. (2012). *Harry Potter and the Sorcerer's Stone*. Pottermore Limited.
- Satopaa, V., Albrecht, J., Irwin, D., and Raghavan, B. (2011). Finding a "kneedle" in a haystack: Detecting knee points in system behavior. In *2011 31st International Conference on Distributed Computing Systems Workshops*, pages 166–171. IEEE.
- Schwarz, G. (1978). Estimating the dimension of a model. *The annals of statistics*, pages 461–464.
- Seghier, M. L. (2013). The angular gyrus: multiple functions and multiple subdivisions. *The Neuroscientist*, 19(1):43–61.
- Seth, A. K., Barrett, A. B., and Barnett, L. (2015). Granger causality analysis in neuroscience and neuroimaging. *Journal of Neuroscience*, 35(8):3293–3297.
- Spencer, D., Guhaniyogi, R., and Prado, R. (2022). Parsimonious Bayesian sparse tensor regression using the Tucker decomposition. *arXiv preprint arXiv:2203.04733*.
- Spiegelhalter, D. J., Best, N. G., Carlin, B. P., and Van Der Linde, A. (2002). Bayesian measures of model complexity and fit. *Journal of the Royal Statistical Society: Series B (Statistical Methodology)*, 64(4):583–639.
- Wang, D., Zheng, Y., Lian, H., and Li, G. (2022). High-dimensional vector autoregressive time series modeling via tensor decomposition. *Journal of the American Statistical Association*, 117(539):1338–1356.
- Wehbe, L., Murphy, B., Talukdar, P., Fyshe, A., Ramdas, A., and Mitchell, T. (2014). Simultaneously uncovering the patterns of brain regions involved in different story reading subprocesses. *PloS one*, 9(11):e112575.
- Weiner, K. S. and Zilles, K. (2016). The anatomical and functional specialization of the fusiform gyrus. *Neuropsychologia*, 83:48–62.

- Xiong, X. and Cribben, I. (2023). Beyond linear dynamic functional connectivity: a vine copula change point model. *Journal of Computational and Graphical Statistics*, 32(3):853–872.
- Zhang, W., Cribben, I., and Guindani, M. (2021). Bayesian time-varying tensor vector autoregressive models for dynamic effective connectivity. *arXiv preprint arXiv:2106.14083*.
- Zhao, Q., Hautamaki, V., and Fränti, P. (2008). Knee point detection in BIC for detecting the number of clusters. In *International Conference on Advanced Concepts for Intelligent Vision Systems*, pages 664–673. Springer.
- Zhou, H., Li, L., and Zhu, H. (2013). Tensor regression with applications in neuroimaging data analysis. *Journal of the American Statistical Association*, 108(502):540–552.

SUPPLEMENTARY MATERIAL

A Basic Notations and Definitions

A tensor \mathcal{A} is a J -th-order tensor if $\mathcal{A} \in \mathbb{R}^{I_1 \times \dots \times I_J}$ with entries $\mathcal{A}_{i_1, \dots, i_J}$ for $i_j = 1, \dots, I_j$. Vectors and matrices correspond to first- and second-order tensors, respectively. Similar to the definition of a diagonal matrix, a tensor is called a J -th-order *superdiagonal* tensor if $I_1 = \dots = I_J = I$ and only its (i, \dots, i) entries are non-zero for $i = 1, \dots, I$. Extracting entries by a selected index from a matrix \mathbf{A} and a tensor \mathcal{A} is akin.

Matricization of a J -th-order tensor ($J > 2$) is an operation that transforms the tensor into a matrix. There are J possible matricizations for a J -th-order tensor \mathcal{A} , and the matricization to the j -th dimension is called the *mode- j matricization* with notation $\mathcal{A}_{(j)} \in \mathbb{R}^{I_j \times \prod_{j' \neq j} I_{j'}}$, where the i_j -th row corresponds to the vectorization of $\mathcal{A}_{\dots, i_j, \dots}$.

The outer (or tensor) product of two vectors $\boldsymbol{\beta}_1 \in \mathbb{R}^{I_1}$ and $\boldsymbol{\beta}_2 \in \mathbb{R}^{I_2}$ is $\boldsymbol{\beta}_1 \circ \boldsymbol{\beta}_2$, yielding an I_1 -by- I_2 matrix with its (i_1, i_2) entry as $\beta_{1,i_1} \beta_{2,i_2}$. Assume we have J vectors with $\boldsymbol{\beta}_j \in \mathbb{R}^{I_j}$ denoting the j -th vector, then the J -way *outer product* of these vectors, $\boldsymbol{\beta}_1 \circ \dots \circ \boldsymbol{\beta}_J$, is a $I_1 \times \dots \times I_J$ tensor, with (i_1, \dots, i_j) entry as $\beta_{1,i_1} \dots \beta_{J,i_j}$. Note that the outer product can also apply to a pair of a vector and a matrix. Assume that the vector is $\mathbf{a} \in \mathbb{R}^K$ and the matrix is $\mathbf{B} \in \mathbb{R}^{M \times N}$. Their outer product, $\mathbf{a} \circ \mathbf{B}$, is a third-order tensor with dimension $K \times M \times N$, and the (k, m, n) entry equals to $a_k B_{m,n}$.

B Marginal DIC in TVP-TVAR

The key term in the marginal DIC is $p(\mathbf{y}_{1:T} \mid \mathbf{b}_{j'}, \boldsymbol{\Omega}, \mathbf{Q}_j)$, which marginalizes $\mathbf{b}_{1:T,j}$:

$$\int p(\mathbf{y}_{1:T} \mid \mathbf{b}_{1:T,j}, \mathbf{b}_{j'}, \boldsymbol{\Omega},) p(\mathbf{b}_{1:T,j} \mid \mathbf{Q}_j) d\mathbf{b}_{1:T,j}. \quad (\text{B.1})$$

Analogous to [Chan and Eisenstat \(2018\)](#), $p(\mathbf{y}_{1:T} \mid \mathbf{b}_{j'}, \boldsymbol{\Omega}, \mathbf{Q}_j)$ has a closed form because of the state-space representations described in Section 3. For $j = 1$ or 3, $\mathbf{y} \mid \mathbf{b}_{1:T,j}, \mathbf{b}_{j'}, \boldsymbol{\Omega} \sim \mathcal{N}(\mathbf{Z}_j \mathbf{b}_j, \mathbf{I}_T \otimes \boldsymbol{\Omega})$, where $\mathbf{y} = (\mathbf{y}'_1, \dots, \mathbf{y}'_T)'$, $\mathbf{b}_j = (\mathbf{b}'_{1,j}, \dots, \mathbf{b}'_{T,j})'$, $\mathbf{Z}_j = \text{diag}(\mathbf{Z}_{1,j}, \dots, \mathbf{Z}_{T,j})$;

$$\mathbf{b}_j \mid \mathbf{Q}_j \sim \mathcal{N}(\mathbf{0}, \mathbf{H}^{-1} \mathbf{S}_j (\mathbf{H}^{-1})'), \text{ where } \mathbf{H} = \begin{pmatrix} \mathbf{I}_{jR} & \mathbf{0} & \dots & \mathbf{0} \\ -\mathbf{I}_{jR} & \mathbf{I}_{jR} & \ddots & \mathbf{0} \\ \vdots & \ddots & \ddots & \vdots \\ \mathbf{0} & \dots & -\mathbf{I}_{jR} & \mathbf{I}_{jR} \end{pmatrix}, \mathbf{S}_j = \text{diag}(\boldsymbol{\Sigma}_j, \mathbf{Q}_j, \dots, \mathbf{Q}_j).$$

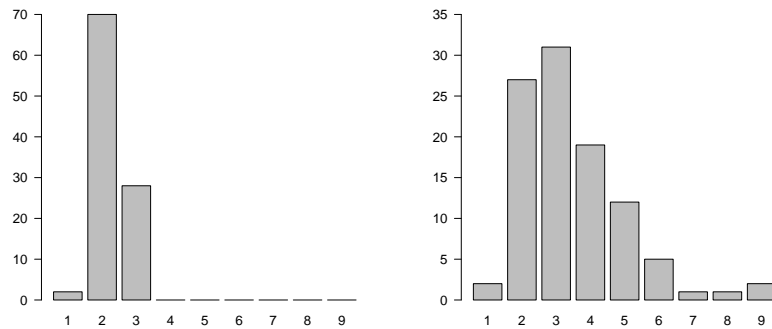
By plugging in the probability density functions of the above two distributions to (B.1), we can get $p\left(\mathbf{y}_{1:T} \mid \boldsymbol{\theta}_{\setminus \mathbf{b}_{1:T,j}}\right) = (2\pi)^{-\frac{TN}{2}} |\boldsymbol{\Omega}|^{-\frac{T}{2}} |\mathbf{Q}_j|^{-\frac{T-1}{2}} |\boldsymbol{\Sigma}_j|^{-\frac{1}{2}} |\mathbf{V}_j|^{-\frac{1}{2}} \exp\left\{-\frac{1}{2} \left[\mathbf{y}' (\mathbf{I}_T \otimes \boldsymbol{\Omega})^{-1} \mathbf{y} - \mathbf{m}'_j \mathbf{V}_j^{-1} \mathbf{m}_j\right]\right\}$,

where $\mathbf{V}_j = \mathbf{Z}'_j (\mathbf{I}_T \otimes \boldsymbol{\Omega})^{-1} \mathbf{Z}_j + \mathbf{H}' \mathbf{S}_j^{-1} \mathbf{H}$, $\mathbf{m}_j = \mathbf{Z}'_j (\mathbf{I}_T \otimes \boldsymbol{\Omega})^{-1} \mathbf{y}$. Thus, $\log p\left(\mathbf{y}_{1:T} \mid \mathbf{b}_{j'}, \boldsymbol{\Omega}, \mathbf{Q}_j\right)$ is written as

$$-\frac{TN}{2} \log 2\pi - \frac{T}{2} \log |\boldsymbol{\Omega}| - \frac{T-1}{2} \log |\mathbf{Q}_j| - \frac{1}{2} \log |\boldsymbol{\Sigma}_j| - \frac{1}{2} \log |\mathbf{V}_j| - \frac{1}{2} \left[\mathbf{y}' (\mathbf{I}_T \otimes \boldsymbol{\Omega})^{-1} \mathbf{y} - \mathbf{m}'_j \mathbf{V}_j^{-1} \mathbf{m}_j\right].$$

For $j = 2$, the expression of $\log p\left(\mathbf{y}_{1:T} \mid \mathbf{b}_{j'}, \boldsymbol{\Omega}, \mathbf{Q}_j\right)$ is the same after modifying \mathbf{Q}_2 according to the order of elements in $\mathbf{b}_{t,2}^*$. We apply the algorithm in Section 3 to sample unknown parameters to approximate the posterior mean deviance.

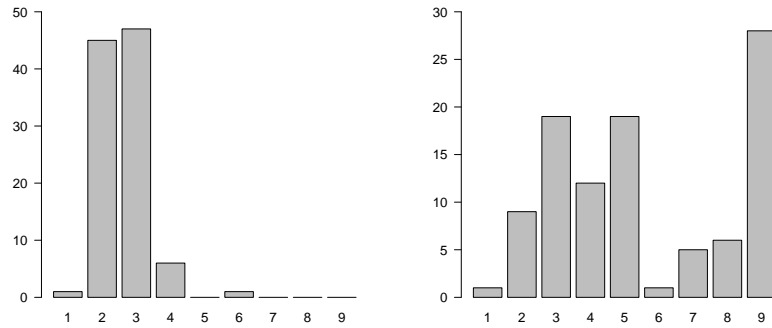
C Additional Results in the Monte Carlo Study



(a) With knee point detection.

(b) Without knee point detection.

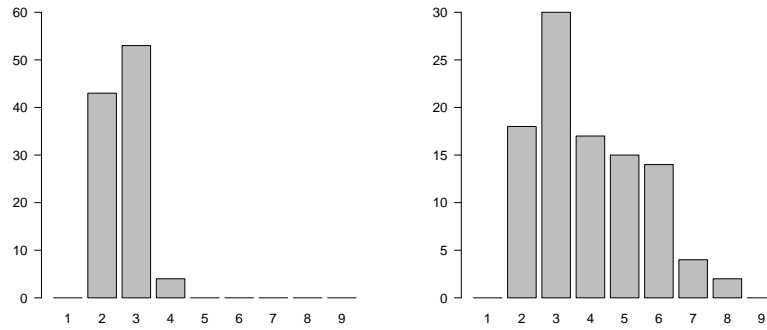
Figure 9: Histograms of selected ranks based on data sets generated from TVAR(3).



(a) With knee point detection.

(b) Without knee point detection.

Figure 10: Histograms of selected ranks based on data sets generated from TVP-TVAR(3,2).



(a) With knee point detection.

(b) Without knee point detection.

Figure 11: Histograms of selected ranks based on data sets generated from TVP-TVAR(3,3).

D Data

ROI	Label
1 Angular gyrus	AG
2 Fusiform gyrus	F
3 Inferior temporal gyrus	IT
4 Inferior frontal gyrus, opercular part	IFG 1
5 Inferior frontal gyrus, orbital part	IFG 2
6 Inferior frontal gyrus, triangular part	IFG 3
7 Middle temporal gyrus	MT
8 Inferior occipital gyrus	IO
9 Precentral gyrus	PCG
10 Precuneus	PC
11 Supplementary motor area	SM
12 Superior temporal gyrus	ST
13 Superior Temporal pole	STP
14 Supramarginal gyrus	SG

Table 4: 27 regions of interest from both right and left cerebral hemispheres, except the supramarginal gyrus for which only the right hemisphere was considered.

References

Chan, J. C. and Eisenstat, E. (2018). Bayesian model comparison for time-varying parameter VARs with stochastic volatility. *Journal of Applied Econometrics*, 33(4):509–532.